

Refining Technology and Low Temperature Properties for High Purity Aluminium

Sumitomo Chemical Co., Ltd.

Basic Chemicals Research Laboratory

Hiroaki HOSHIKAWA

Ichiro TANAKA*

Tomohiro MEGUMI

High purity aluminium is widely used in electronics applications such as electrolytic capacitor foils, hard disk substrates, wiring materials in semiconductors utilizing its controllability of oxide layer and its absence of impurities or inclusions. It is also used as an electrical and thermal conductor for superconducting magnets at low temperatures. Here the recent progress in refining technologies for high purity aluminium and its physical properties and applications at low temperatures are shown.

This paper is translated from R&D Report, "SUMITOMO KAGAKU", vol. 2013.

Introduction

High purity aluminium is used for a wide range of electronics applications, including anode foils for aluminium electrolytic capacitors, hard disk substrates, bonding wires, and wiring materials for semiconductors and liquid crystal display panels, due to the following reasons: Oxide films having excellent permittivity and insulation properties can be obtained through surface treatment; high purity aluminium contains only a small amount of impurity elements, precipitates and inclusions; and it has high electrical and thermal conductivities. In recent years it has been used in stabilized superconductors and thermal conductors, making the most of its outstanding properties, which can be demonstrated at low temperatures.

Sumitomo Chemical is one of the world's leading producers of high purity aluminium. For many years our technology and quality has been highly valued by our customers. This paper introduces the refining processes, low-temperature properties and application examples of high purity aluminium.

Refining Processes

The purity of primary aluminium manufactured using the Hall-Héroult process generally ranges from 99.5% to

99.9%. However, an additional refining process is required for the production of high purity aluminium having even higher purity. The major refining processes currently used in Japan and other countries are the segregation process and the three-layer electrolytic refining process (three-layer process). Through those processes, high purity aluminium having a purity of 99.98% or greater is manufactured. Additionally, the most commonly used notations for purity are 4N (four-nine) for 99.99% and 4N8 (four-nine-eight) for 99.998%.

Ultra high purity aluminium having a purity of 5N or higher (SUPRAL[®]) is used for sputtering targets to fabricate wiring materials for semiconductors, as well as for liquid crystal display panels, stabilizers for superconductors and thermal conductors. For the aluminium manufacturing methods used to achieve such high purity levels, the three-layer process, zone refining process and organic aluminium electrolytic refining processes are generally known, as are the combinations of those techniques. Accompanied by the recent progress in analytical techniques, new refining techniques have been developed. In this paper we will explain the major refining processes.

1. Three-Layer Electrolytic Refining Process (Three-Layer Process)

The molten salt electrolytic process for refining aluminium was begun as a trial by the U.S. researcher W. Hoopes in 1901. This technique was industrialized in 1919 by Alcoa. Subsequent to its initial industrialization,

* Currently: Aluminium Division and Basic Chemicals Research Laboratory

its cell structure, method of operation and electrolyte composition have been repeatedly improved by engineers in many countries, and in turn the current three-layer process has been established. In Japan, our company (former Sumitomo Aluminium Smelting Co., Ltd.) succeeded in its industrial operation and, in 1942, began manufacturing high purity aluminium having a purity of 99.99%.^{1), 2)}

Fig. 1 shows the structure of a three-layer electrolytic refining cell. High purity aluminium is manufactured through an electrolytic refining process in which the anode alloy layer, electrolyte layer and cathode (refined) aluminium layer are retained at a specific gravity difference in a refining cell. The bottom layer of the anode alloy is composed of aluminium alloy containing 30% to 40% of copper, and its specific gravity is approximately 3.0g/cm^3 . Because the aluminium contained in the anode alloy is electrolytically transported to the cathode layer, it is necessary to charge the raw aluminium to the anode alloy layer at an amount equal to the deposition. The specific gravities of the aluminium in the middle layer (i.e. the electrolytic bath) and the top layer (i.e. refined cathode aluminium) are approximately 2.7g/cm^3 and 2.3g/cm^3 , respectively.

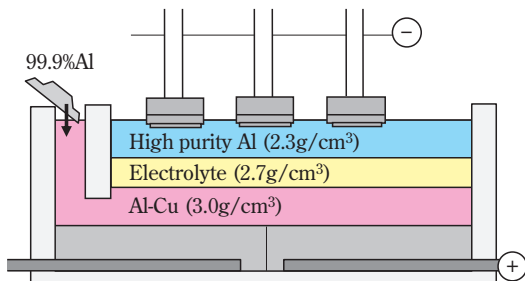


Fig. 1 Schematic diagram of three-layer electrolytic refining process

The electrolyte plays the most important role in the electrolytic refining process and has the following conditions:

- It has a specific gravity between those of the anode alloy and the cathode aluminium;
- It is a metallic salt which is more active than aluminium;
- It has a low melting point and a low volatilization loss and it is chemically stable; and
- It has high electrical conductivity.

The electrolytic baths that fulfill the above conditions are ones that utilize fluorides, chlorides or mixed salts

of Na, Ba, Al, Ca and Mg. Of those elements, Ba salts are chosen to enlarge the specific gravity.

We at Sumitomo Chemical have significantly reduced impurities such as Fe, Si and many others through the implementation of measures to prevent inclusions, quality assurance of various raw materials and furnace materials, and computerized operation control. Consequently, we have achieved purity of 5N or greater.

2. Segregation Process

The segregation process is a purification method based on the segregation phenomenon that occurs upon the solidification of alloys. This method was industrialized during the second half of the 1970s. Beginning in 1981, several companies in Japan (including Sumitomo Chemical) industrialized the segregation process using their own proprietary technologies. The segregation process can be roughly classified into fractional crystallization, unidirectional solidification and some other methods.³⁾ Our company uses the unidirectional solidification method.

In a binary alloy system when the ratio between the impurity concentration C_L of the liquid phase and the impurity concentration C_S of the solid phase in equilibrium is expressed using the equilibrium distribution coefficient $K=C_S/C_L$, by cooling the molten aluminium containing so-called the eutectic impurity elements having K smaller than 1 (such as Fe or Si), purified primary crystals with the impurity concentration KC_0 (C_0 : initial impurity concentration) will be produced. Purification is achieved by isolating such primary crystals from the remaining liquid (Fig. 2).

Conversely, because the so-called peritectic impurity elements having K larger than 1 (such as Ti, Cr and Zr) become concentrated in the solid phase, B is commonly added prior to the segregation process to separate the peritectic elements as borides.

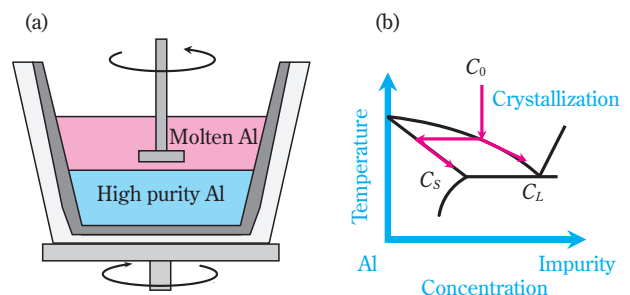


Fig. 2 (a) Schematic diagram of segregation process and (b) phase diagram

During the equilibrium solidification, the solidification of the eutectic alloy having an initial impurity concentration of C_0 begins at $K C_0$. The solidification progresses while discharging solute elements into the liquid phase. However, in the unidirectional solidification used in practical situations, an impurity-concentrated layer is formed in the liquid phase in the vicinity of the solid-liquid interface, thus causing the impurity concentration in the solid phase to become higher than that of the equilibrium solidification. When this occurs, assuming that the impurity concentrations of other liquid phases (except for the impurity-concentrated layer) are constant due to convection or other reasons, the apparent distribution coefficient (K_e : effective distribution coefficient) can be expressed using the formula shown below:

$$K_e = \frac{C_S}{C_0} = \frac{K}{K + (1-K) \cdot \exp(-R\delta/D_L)} \quad (0 < K < K_e < 1) \quad (1)$$

R : Solidification rate

δ : Thickness of the impurity-concentrated layer

D_L : Diffusion coefficient of the solute element in the liquid phase

It is effective to reduce the solidification rate and the thickness of the impurity-concentrated layer in order to allow K_e to become closer to K . Because a reduction of the solidification rate will in turn reduce the productivity, in the production process producers attempt to reduce the thickness of the impurity-concentrated layer by mechanical stirring of the liquid phase or other methods.

Fig. 2 shows the schematic diagram of our company's refining process. Molten aluminium is poured into a crucible. While rotating the crucible and heating and stirring the upper part of the molten aluminium, the refined aluminium is sequentially solidified from the bottom. Once a certain amount of refined aluminium has been solidified, the remaining molten aluminium containing a lot of impurities is discharged, whereupon the remaining solidified high purity aluminium is retrieved from the crucible. Generally, in comparison to the three-layer process described above, the segregation process for high purity aluminium production requires a smaller capital investment and manufacturing costs are also smaller due to low power consumption. However, the purity of aluminium obtained through the segregation process depends on the purity of the raw material, and it usually ranges from approximately 3N8 to 4N5. Such high purity aluminium is mainly used as the raw materi-

al for anode foils in aluminium electrolytic capacitors and for hard disk substrates.

3. Ultra-high Vacuum Melting Refining Process

The aluminium refining method by which high purity aluminium is melted in an ultra-high vacuum is called ultra-high vacuum melting. The principle thereof is generally assumed to be based on the difference in saturated vapor pressure between the aluminium and the impurity elements.

This section describes the results of ultra-high vacuum melting performed on our company's 6N aluminium, of which industrial mass production has been successfully achieved:^{4), 5)}

First, the raw material was processed into a pillar shape. The pillar was then positioned in a cooled crucible in the vacuum chamber. Subsequently, the material was melted in an ultra-high vacuum by high-frequency heating, which was maintained for a predetermined time. The material was solidified by gradually decreasing the power of high-frequency heating. The degree of vacuum reached before the point of melting was 3×10^{-8} Pa, and the degree reached during melting was $3 \sim 6 \times 10^{-6}$ Pa.

Fig. 3 shows the appearance and a cross section of the melted sample. Position F and the areas above F are the more refined areas due to vacuum melting, and coarse crystal grains have been obtained from those areas by slow cooling. Given the high purity of 5N or greater, the number of ingredients of which the quantity is lower than the detection limit for impurity analysis would increase. Therefore, marking of the total impurities can be difficult in some cases. For this reason the residual resistivity ratio (RRR) is often used as an index of high purity. To explain it briefly, RRR is a ratio of the electrical conductivity at a low temperature (generally 4.2K) to that at room temperature. The purer the material is, the higher the ratio will be. Because RRR does not depend on evaluation equipment and can be conveniently used, it is widely used as a purity index. An RRR sample was collected from each position and the RRR values were measured after annealing to relieve stress. **Fig. 4** indicates the results of the RRR measurement of the samples. Additionally, the values obtained after conducting a size-effect correction—which will be described later—are expressed as RRR_b . Furthermore, the residual resistivity ratio analyzed based on the results of the impurity analysis conducted on each position is also shown as RRR_e . The tendencies of RRR_b and RRR_e are

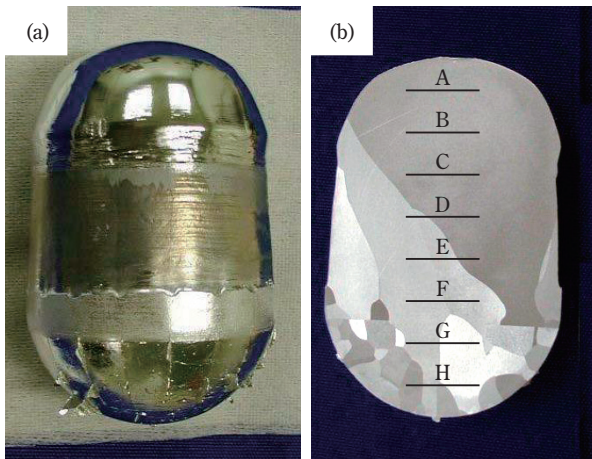


Fig. 3 Aluminium ingot purified through ultrahigh-vacuum melting. (a) Photographs and (b) cross section of etched surface. A-H show the sample positions for composition analysis and resistivity measurements.⁴⁾

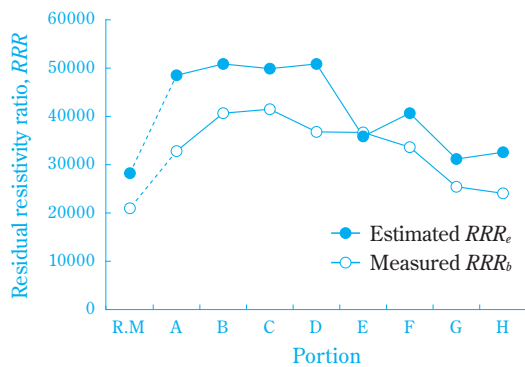


Fig. 4 Measured and estimated residual resistivity ratio for ultrahigh-vacuum melted aluminium. R.M. shows the raw material.⁴⁾

consistent, and the area from position A to position F has been refined better than the raw material indicated as R.M. The RRR_b of position B was approximately 40,000, which was approximately twice as large as that of the raw material. Positions G and H were thought to be the regions which had been solidified by coming into contact with the cooled crucible immediately after melting, and in those positions no remarkable purification effects were achieved. As a result of impurity analysis conducted using glow discharge mass spectrometry (GDMS), the total value of Si, Fe and Cu was 0.2ppm or smaller in well refined regions.

A significant characteristic of this refining method is the fact that a high purification effect can be achieved within a relatively short period of time. It is particularly effective for the reduction of elements having a large

saturated vapor pressure, such as Mg. Furthermore, it can be theoretically surmised that this method can effectively reduce gaseous ingredients such as C, O and N. However, it is necessary to further examine this area, including the analysis method.

4. Zone Refining Process

After melting one side of a long, slender raw material, if the melting part is slowly moved toward the other end of the material either by moving the material itself or moving the heating mechanism, the impurity elements will move toward the same end based on the same principle of the segregation process. This technique for refining other zones of the raw material (except for the melting end) is called the zone refining process. The melting operation can be performed only once, or it can be repeated to enhance the purification effect. The raw material can be positioned horizontally or vertically. For the heating mechanism, several techniques—such as resistance heating, high frequency induction heating and optical heating—can be utilized. Although the zone refining process is suitable for small-quantity production due to its lengthy refinement time, high purity exceeding 6N can be achieved by using high purity aluminium obtained through the three-layer process as the raw material.

We will now describe the results of the purification experiment conducted on our company's aluminium having a purity of 6N.⁶⁾ The raw material was processed into a square pillar having a length of 900 mm. The pillar was then positioned on a graphite boat and heated using a high-frequency coil. The zone refining was performed by moving the melting part by 5 or 10 passes. The purified sample was then cut up at even intervals, after which RRR was measured and the impurities were analyzed at each black-dotted point as shown in Fig. 5. Additionally, the RRR values were organized with the RRR_b values, which were obtained after the correction of the size effect (described later).

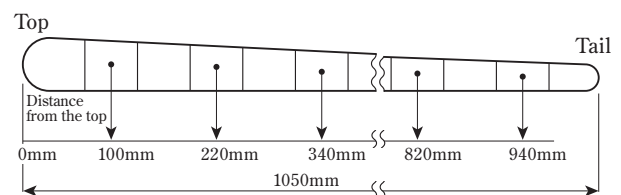


Fig. 5 Sample positions for resistivity measurement and composition analysis in purified aluminium through zone refining process⁶⁾

Fig. 6 shows the results of the *RRR* measurements. Because impurities such as Si, Fe and Cu moved toward the final melt zone (the tail zone) and concentrated there, the *RRR* values at the final melt zone became lower than 21,000, which was the value of the raw material. It can be observed that *RRR* values exceeding that of the raw material were achieved over a broad area outside the final solidification zone, and thus it became refined. Some elements such as Ti moved toward the point where melting had started (the top zone), and consequently the area near the center of the material became refined most adequately, thus achieving high *RRR* values in excess of 50,000. Additionally, the sample ZR-04 had half of the moving velocity of the melt zones ZR-01 and -02, and by decreasing the moving velocity (i.e. prolonging the refining time) the purification effect was further improved.

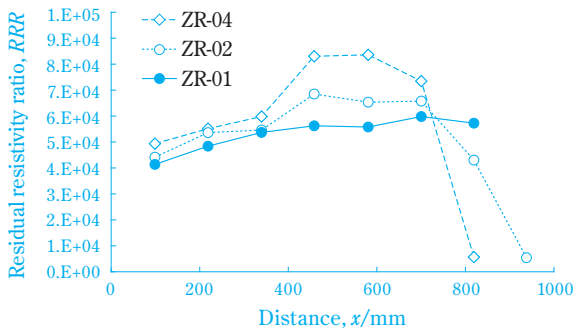


Fig. 6 Measured residual resistivity ratio for zone-refined aluminium. Zone speed was 60 mm/h for ZR-01 and ZR-02, and 30 mm/h for ZR-04.⁶⁾

The study on simulation techniques for more efficient investigation into purification conditions is progressing as well. In this study, based on the solidification model known for quite some time,⁷⁾ the manner in which the concentration in the melting side and that in the solid phase side at the solidification interface change according to the movement of the melt zone is observed. Here, the method by which to evaluate the thickness of the impurity-concentrated layer and the concentration gradient in this layer is crucial because, in the melt zone, the impurity-concentrated layer and the stirring zone are present.

First, in the stirring zone it is assumed that the impurity concentration is constant. The degree of impurity in the concentrated layer can be expressed using an exponential function. It is assumed that it can be handled as a constant value, and thus a simplified model is

introduced. Accordingly, the thickness of the impurity-concentrated layer was obtained through a comparison with the GDMS impurity analysis results, and the purification effect of each element was simulated.

Fig. 7 shows the results of the impurity analysis and the simulations for Ti and Si. The phenomena whereby the elements having a distribution coefficient larger than 1 move toward the starting point of the melting process, while those having a distribution coefficient smaller than 1 move toward the zone where the melting process has been completed, were also reproduced in the simulation. Additionally, the simulation values and analysis values were very consistent. Furthermore, regarding Mg, the result of impurity analysis was significantly smaller than the simulation result. It can be surmised that this is because Mg became evaporated and disappeared *in vacuo* due to its high vapor pressure. Because those results indicate that the purification behaviors of a large number of elements (except for Mg) can be successfully evaluated and that the effects of experimental conditions such as the number of passes can be examined through this simulation, it can be concluded that this simulation technique is an effective tool.

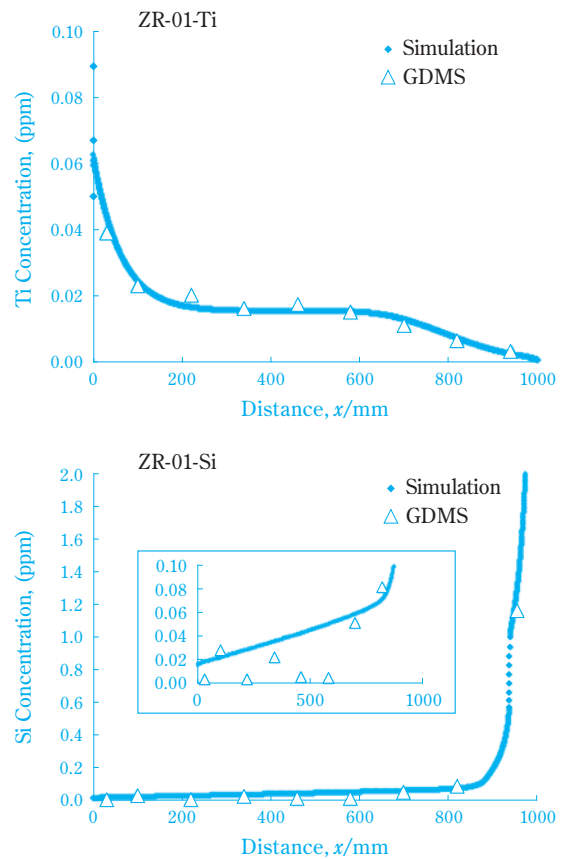


Fig. 7 Composition profile and analysis results for Ti and Si⁶⁾

About Low-Temperature Properties

We have thus far explained the techniques to increase the purity of aluminium. There are several properties that will change along with the purification. Of such properties, those that will show a remarkable change are electric and thermal conductivities at low temperatures. In proportion to the improvement of purity, the electric and thermal conductivities will increase. Particularly, high purity aluminium shows extremely high conduction properties at low temperatures, as is the case with aluminium used in the field of superconductors (temperatures below 30 K are also referred to as cryogenic temperatures). As with oxygen-free copper (high purity copper), which is well known as a thermal conductor at low temperatures, it is useful as a peripheral member in superconducting magnets. Occasionally, high purity aluminium is positioned in the magnetic field upon application. Thus the physical-property change in the magnetic field is important. Furthermore, when aluminium reaches high purity, the effect of the sample size on conductivity increases. It is therefore important to understand such a phenomenon. Below we will describe the low-temperature properties, mainly by focusing on the evaluation results of our company's high purity aluminium.

1. Temperature Dependency of Conduction Properties

The conduction properties of aluminium change significantly in the temperature zone ranging from low up to room temperature. Particularly, in high purity aluminium the conductivity can become 10,000 times greater. In order to understand and make the most of such conductivity over a broad temperature range, as well as the electrical resistivity, which is its inverse, it is essential to understand the factors of electrical resistivity. The electrical resistivity factors include phonon, impurity elements (chemical impurities), surface scattering, point defects, line defects (dislocations) and plane defects (grain boundaries and stacking faults),⁸⁾ and it has been known as Matthiessen's Rule that the resistivity components of each factor are countable. Generally, the effects of phonon and impurity elements are large.

A phonon is a quantum of lattice vibration energy. Lattice ions in aluminium crystals are arranged with periodicity and thermally vibrate around the equilibrium position. The quantized lattice vibrations are called

phonons. As seen in the schematic diagram (Fig. 8) of the aluminium temperature and electrical resistivity, which have been known for many years, phonons are the dominant factor in the electrical resistivity around room temperature. Therefore, even though the aluminium purity differs, the change in the electrical resistivity around room temperature is relatively small.

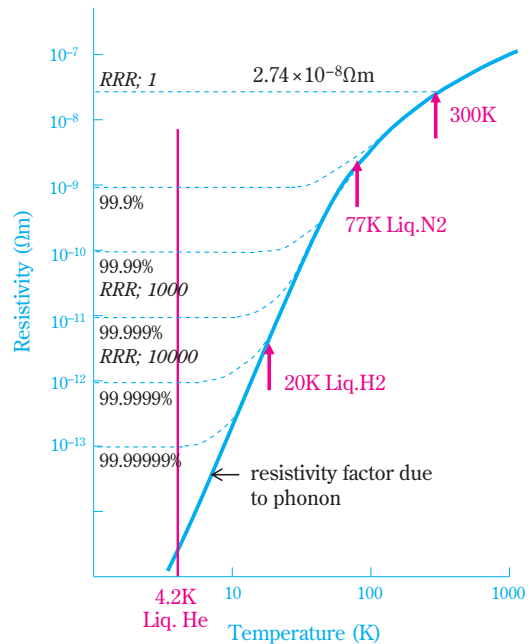


Fig. 8 Schematic diagram of aluminium purity dependence on specific resistivity

When temperature drops, the contribution of phonons to the electrical resistivity suddenly declines, thereby reducing the electrical resistivity. The effect of phonons can be ignored at low temperatures such as the 4.2K of liquid helium, and instead the impurity elements become the principal factor in electrical resistivity. Therefore, the higher the purity is, the smaller the electrical resistivity will be. One can understand that when the effects of other factors such as point defects, line defects and surface scattering can be ignored, if the purity improves by one digit, the electrical resistivity at a low temperature will decrease by one digit.

In reality, the resistivity will be inconsistent with that shown in the schematic diagram if the aluminium purity is extremely high due to the following reasons: The effects of impurity elements on the electrical resistivity vary depending on the elements; the sample size is limited; and the effects of other crystal defects cannot be ignored. Therefore, we have measured the electrical resistivity of our company's high purity aluminium

sheets. The following aluminium sheets, each having a thickness of 0.5mm, were prepared: 2N7, 4N, 5N and 6N that could be industrially mass produced; 6N7 manufactured through the zone refining process; and the comparison material 5N-Cu. Next, these aluminium sheets were annealed *in vacuo* in order to remove strain. The electrical resistivity of these sheets was measured at temperatures ranging from 4.2 K up to room temperature. Consequently, while the differences in resistivity among the sheets having different purities were minimal at room temperature, such differences were considerable at low temperatures, according to

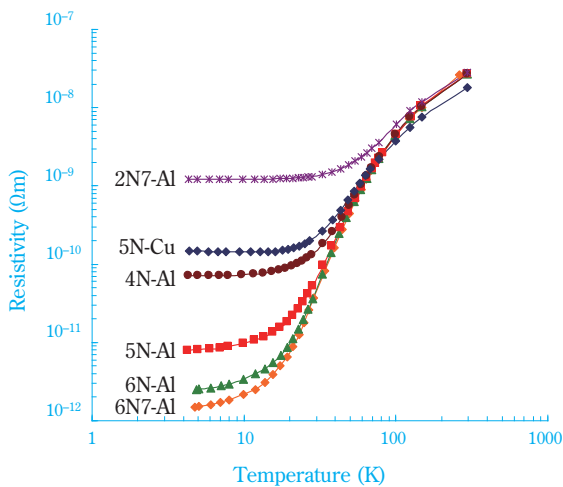


Fig. 9 Measured specific resistivity for high purity aluminium and copper using 0.5 mm thickness sheet annealed at 773 K

the purity of the aluminium (**Fig. 9**). Moreover, while the electrical resistivity of 5N-Cu was lower than that of high purity aluminium sheets at room temperature, at low temperatures 5N-Cu showed higher resistivity than the high purity aluminium sheets having a purity of 4N or greater.

2. Conduction Properties in a Magnetic Field

The magnetoresistance effect is the phenomenon by which the electrical properties of a metal change in a magnetic field. Materials for use at low temperatures are occasionally exposed to magnetic fields. For example, a clinical MRI generally uses magnetic fields ranging from 0.5 to 3 tesla, and an analytical NMR uses even higher magnetic fields. Therefore, the physical properties in a magnetic field are important. It has been known that the tendency of the magnetoresistance effect varies between bivalent metals such as Cu and metals having odd-number valences, such as Na and Al. Although the measurement of the magnetoresistance of aluminium has been reported by Lutes, Stevenson and Hartwig, et al.,^{9)–11)} there is no sufficient measurement data regarding high purity aluminium, which has recently become industrially available. Thus we will report the recent evaluation of our company's aluminium.¹²⁾

In order to evaluate the transverse and longitudinal electrical properties, two types of quartz jigs were prepared (**Fig. 10**).

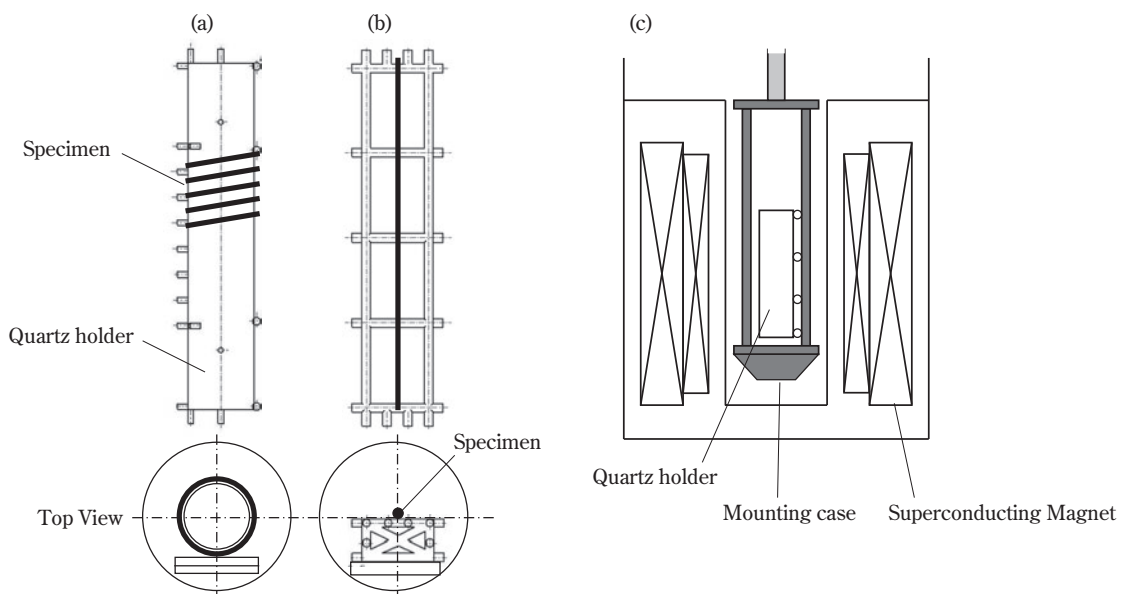


Fig. 10 Diagrams of quartz holders with samples for measuring transverse magnetoresistance (a) and longitudinal magnetoresistance (b), along with geometry of quartz holders, sample mounting case made of GFRP, and superconducting magnet (c).¹²⁾

Table 1 Chemical compositions of 5N, 6N, and 6N8-Al (wt-ppm)

| | Si | Fe | Cu | Mg | Mn | Zn | Ti | Ga | Total 1*1 | Total 2*2 |
|--------|-------|---------|-------|---------|-------|---------|-------|---------|-----------|-----------|
| 5N-Al | 2.3 | 0.60 | 1.1 | 0.48 | 0.007 | 0.22 | 0.060 | 0.006 | 4.0 | < 4.8 |
| 6N-Al | 0.34 | 0.089 | 0.14 | 0.10 | 0.004 | 0.002 | 0.027 | 0.001 | 0.57 | < 0.71 |
| 6N8-Al | 0.003 | < 0.001 | 0.016 | < 0.001 | 0.006 | < 0.001 | 0.031 | < 0.001 | < 0.020 | < 0.060 |

*1: sum of Si, Fe, and Cu,

*2: sum of Si, Fe, Cu, Mg, Mn, Zn, Ti, and Ga.

First, high purity aluminium wires with chemical compositions shown in **Table 1** were created and fixed onto the quartz jigs. Next, in order to remove strain that occurred during the process, annealing at 773K was performed, then the quartz jigs were fixed onto a holder made of glass fiber reinforced plastic (GFRP). This system was then fixed onto a superconducting magnet and soaked in liquid He, whereupon the *RRR* values were measured in the magnetic field. **Fig. 11** depicts the electrical resistivity measurement results observed when a magnetic field was applied to the sample vertically (transverse magnetoresistance). When a relatively low magnetic field up to 0.5 tesla was applied, the electrical resistivity increased significantly. Furthermore, in high magnetic fields the changes to the electrical resistivity became smaller, and the resistivity between 0.5 and 15

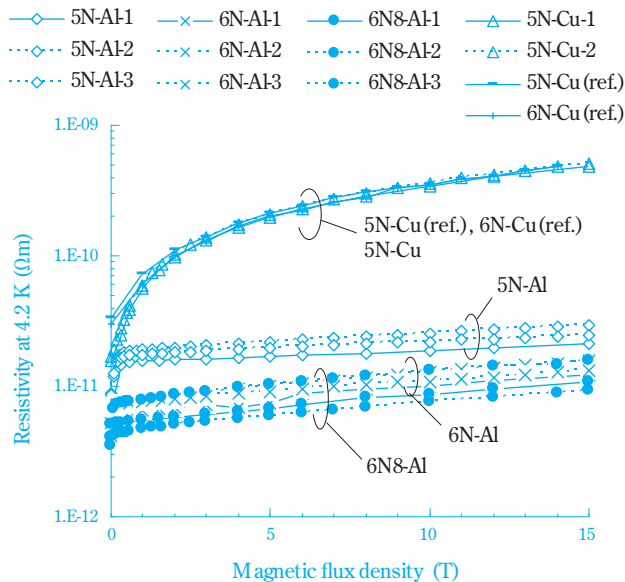


Fig. 11 Transverse magnetoresistance at 4.2 K of 0.5-mm-diameter-specimens. Dashed lines show the results obtained using the delta mode method, while solid lines show the results obtained from the use of a DC current source. The literature data are also plotted for comparison as 5N-Cu(ref.) and 6N-Cu(ref.).¹²⁾

teslas showed a tendency toward saturation. The result from the measurement of the 5N-Cu wire, which was performed in the same manner for the purpose of comparison, and the literature data of 5N-Cu and 6N-Cu¹³⁾ are also shown in the figure. It can be observed that the experimental data and the literature data are mutually consistent. The behavior of the magnetoresistance effect of the high purity copper differs from that of aluminium, and the electrical resistivity increased monotonously without becoming saturated toward the magnetic field.

Table 2 shows the measurement results of the electrical resistivity observed when the magnetic field was horizontally applied to the sample (longitudinal magnetoresistance), as well as the previously described transverse magnetoresistance measurement results. As with the transverse magnetoresistance, the magnetoresistance behavior differed between aluminium and copper. In the longitudinal magnetoresistance measurements, the increase in electrical resistivity due to the magnetic field (i.e. magnetoresistance effect) was smaller than that for the measurement of transverse magnetoresistance. Furthermore, in aluminium having purities of 6N and 6N8, the electrical resistivity became smaller in high magnetic fields (i.e. the negative magnetoresistance effect). This phenomenon can be explained as follows: The conduction electrons move in a screw-like motion due to the effect of the magnetic field, thus minimizing the effect of electron scattering on the sample surface.

Table 2 *RRR* of high purity aluminium and copper at 0 T and 15 T¹²⁾

| purity | diameter (mm) | transverse | | longitudinal | |
|--------|---------------|------------|------|--------------|------|
| | | 0 T | 15 T | 0 T | 15 T |
| 5N-Al | 0.5 | 4100 | 1300 | 3700 | 2500 |
| | 1.0 | 3800 | 1000 | 5800 | 3000 |
| 6N-Al | 0.5 | 6400 | 2200 | 7600 | 7000 |
| | 1.0 | 7300 | 2300 | 11000 | 7800 |
| 6N8-Al | 0.5 | 6600 | 2500 | 8100 | 9400 |
| | 1.0 | 8600 | 3600 | 11000 | 9000 |
| 5N-Cu | 0.5 | 1100 | 36 | 1100 | 240 |

As seen in these results, high purity aluminium maintained an RRR of 1,000 or greater even in high magnetic fields, and demonstrated extremely high conduction properties.

3. Sample Size Dependence of Conduction Properties (Size Effect)

Materials for use at low temperatures have various shapes such as ingot-mass materials, sheet materials and wire materials. For example, as with aluminium having a purity of 4N, for materials having an RRR of 500 or lower, there is nearly no need to consider the effect of the shape on the conduction properties. However, with materials having a purity of 5N or greater, or those for which the RRR exceeds several thousands, the effect of the shape cannot be ignored: the thinner the sample sheet or wire is, the lower the conductivity will be.

This phenomenon is referred to as the size effect. The size effect has a correlation with surface scattering, which is one of the electrical resistivity factors of metals, and it can be caused by the inelastic scattering of free electrons (i.e. carriers) that occurs when those electrons collide with the sample surface. The ratio of the occurrences of inelastic scattering and elastic scattering varies depending on the material. It has been experimentally shown that inelastic scattering occurs in aluminium.^{14), 15)}

Here we will describe an experiment conducted in order to quantitatively evaluate the relationship between purity and the size effect. Wire materials having different diameters were created using our compa-

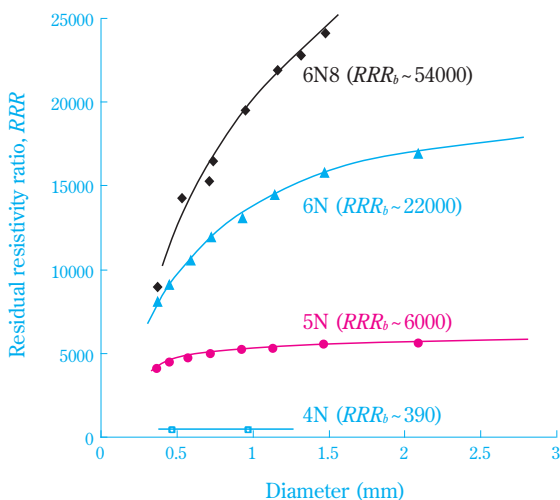


Fig. 12 Measured RRR values using high purity aluminium wire specimens annealed at 773 K

ny's 4N, 5N, 6N and 6N8-Al, which were created through the zone refining process. After removing the surfaces with acid, annealing was performed in order to remove strain that occurred during the process. The RRR values of these wire materials were measured and plotted against the wire diameters (Fig. 12). Even with the same wire diameter, the higher the purity of the material is, the larger the inclination of the graph will be, and this dynamic clearly reveals the size effect. As the purity increases, RRR will also increase and the size effect will tend to manifest. Therefore, it can be concluded that when it is desirable to allow the conduction properties originally possessed by the bulk material to manifest sufficiently, it is ideal to use a relatively large material.

The size effect of sheet materials—which are very important due to their practicality—was also examined through RRR measurements. For the samples on which RRR measurements may be difficult to perform, RRR values were calculated using the Fuchs-Sondheimer formula.^{16), 17)} The material constant required for this calculation can be evaluated by plotting the inverse of the diameter to the horizontal axis and the logarithm of RRR to the vertical axis based on the previously described results of the experiment on wire materials. Table 3 indicates the evaluation results obtained as described above. For sheet materials having a purity of 4N, because the size effect is minimal, it can be usually ignored. On the contrary, for high purity aluminium sheets having a purity of 5N or greater, their shapes must be taken into account. The sheet thickness measured when the RRR value decreases to 80% of the RRR value for bulk material (RRR_b) was expressed as the “critical thickness.” This value was approximately twice as great as the mean free path of the carrier electrons (which was calculated separately). The thickness of the sheet that may be affected by the size effect can be

Table 3 Size effect for high purity aluminium sheet. RRR_m shows measured RRR values using 0.5 or 1 mm thickness sheets, and denotation * shows calculated values using different measurement results.

| purity | RRR_m /0.5 mm | RRR_m /1 mm | RRR_b | critical thickness |
|--------|--------------------|------------------|---------|-----------------------|
| 4N-Al | 383* | 386* | 389 | 0.02 mm |
| 5N-Al | 5000 | 5300 | 6000 | 0.32 mm |
| 6N-Al | 12000 | 15000 | 22000 | 1.3 mm |
| 6N8-Al | 26000* | 36000* | 54000 | 2.8 mm |

obtained from the mean free path of the carrier electrons. Therefore, one can say that when using a sheet having the same thickness as the above thickness or a thinner sheet, the size effect should be considered.

4. Thermal Conductivity

Due to the dissemination of compact refrigerators, there are increasingly cases in which low-temperature devices are conduction cooled. Thus, taking advantage of materials having outstanding thermal conductivity is an important theme in the design of a cryogenic system. Because high purity aluminium and copper generally demonstrate extremely high thermal conductivity at low temperatures, and because their workability and availability are also excellent, they are often used as thermal conductors for low-temperature devices.

Generally, the thermal carriers of normal metals are electrons, and the thermal conductivity κ is determined by the specific heat, the average velocity and the mean free path of electrons. The temperature dependence of electrons' mean free path varies depending on the scattering mechanism received by electrons. At low temperatures where phonon abundance is adequately small (e.g., 4K), impurities or defects within the metal cause electrons to scatter, thereby determining the electrons' mean free path. Moreover, it has been known that the specific heat at such low temperatures depends on the temperature. Under such circumstances the Wiedemann-Franz law, which claims that the mathematical product of electrical conductivity and temperature are proportional to thermal conductivity, can be established. In the temperature range where the temperature is slightly higher than that described above and the presence of phonons having high energy cannot be ignored, the electron scattering due to phonons becomes dominant, thus invalidating the Wiedemann-Franz law. Given these facts, the thermal conductivity at low temperatures has a temperature dependence, which can be expressed as the following formula: $\kappa = 1/(\alpha T^2 + \beta/T)$. In this formula α and β are constants that can vary according to the material.

Regarding the metals that are important as thermal conductors for use at low temperatures, the thermal conductivities of the 1000 series alloys of pure-aluminium have been presented by Woodcraft.¹⁸⁾ Furthermore, for high purity aluminium and copper, the following formulae have been presented in experiments conducted by Kasahara et al., using 5N-Al and other types of aluminium.^{19), 20)}

$$\kappa(\text{Al}) = \frac{1}{1.8 \times 10^{-7} T^2 + 1.1/RRR/T} \quad \text{for aluminium} \quad (2)$$

$$\kappa(\text{Cu}) = \frac{1}{6.2 \times 10^{-8} T^{2.4} + 0.53/RRR/T} \quad \text{for copper} \quad (3)$$

The above formulae can be established in a temperature range from the superconducting transition temperature (1.2K for aluminium) to approximately 30K.

Recently, Tomaru et al. measured the thermal conductivities of our company's 6N-Al, and formula (2) was verified. Thus we will describe the results of this measurement and verification.²⁰⁾ The thermal conductivity of a strip-shaped sample ($t0.5\text{mm} \times w2.5\text{mm} \times L150\text{mm}$) was measured using the Longitudinal Heat Flow Method (Fig. 13). The square indicates the result using a sample annealed for an hour at 773K, and the circle indicates one annealed for three hours at 773K. The thermal conductivities of the two samples were very consistent, and the RRR values converted from the thermal conductivities were 10,000 and 11,000, respectively. The measured RRR of the same material was 12,500. The thermal conductivity calculated using this value through formula (2) is shown as a solid line in the figure. The result is consistent with the measured thermal conductivity. The thermal conductivity peak is present somewhere around 6K, and an extremely high peak value of 40,000W/m/K has been achieved.

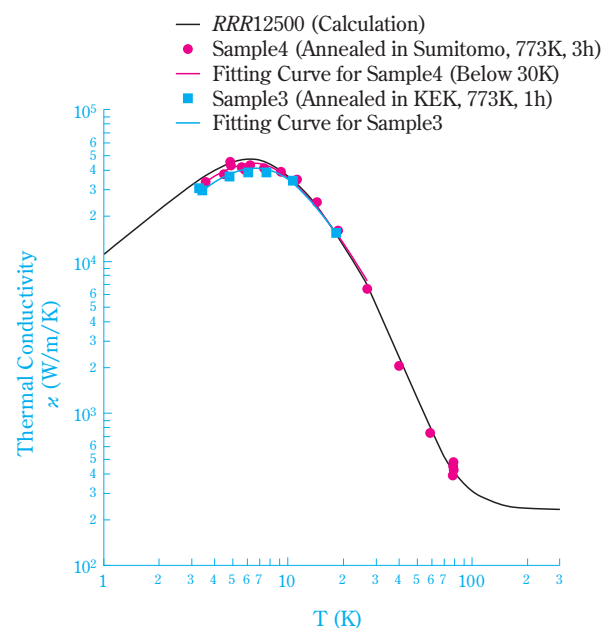


Fig. 13 Measured results for the thermal conductivity of 6N aluminium annealed at 773 K²⁰⁾

5. Applications in Low Temperature Fields

As described thus far, because high purity aluminium has extremely high conduction properties, it can contribute to the improvement of the performance and the reduction of the component's weight, as well as to space saving, when used as a thermal conductor for peripherals of superconducting magnets. A high purity aluminium sheet having a purity of 5N and a thickness of 1.2mm was used as a thermal conductor for the ATLAS detector for the Large Hadron Collider (LHC) at CERN (European Organization for Nuclear Research).²¹⁾ The high purity aluminium was used for the soaking of the superconducting magnet by taking advantage of the aluminium's high thermal conductivity, thus firmly preventing the occurrence of a sudden fracture event (quenching) in the superconductive state.

High purity aluminium also plays an important role as a thermal conductor for low temperatures in the gravitational wave telescopes used to detect gravitational waves from the universe. The Young's modulus of high purity aluminium at 8K is 40GPa, which is lower than that of high purity copper (130GPa). Therefore, high purity aluminium is an important material that can demonstrate high thermal conductivity without transmitting vibrations from the surrounding environment.^{19), 20)}

Metal superconductors for practical use have such a structure that, in order to prevent the occurrence of quenching, extremely thin superconducting wires with multiple cores are wrapped in a metal with high conductivity for the purpose of stabilization. High purity aluminium is used as a stabilizer for this purpose as well. Mechanical strength is often required for thinner and lighter superconducting magnets. In such a case, a slight amount of reinforcing element is added to the high purity aluminium.

The ATLAS and CMS detectors of CERN utilize high purity aluminium-based stabilizers for superconductors.

Because high purity aluminium has the advantage of a lower weight than oxygen-free copper, it demonstrates performance which is suitable for use in light-weight cryogenic components in the field of space observation, such as those for satellites and balloon experiments. In the BESS (Balloon-borne Experiment with a Superconducting Spectrometer) conducted in the Antarctic, a high purity aluminium-based stabilizer was used to achieve light weight.²²⁾

The application of superconducting magnets for industrial use has increased with each passing year. For example, clinical MRIs are not only used in developed countries but are also spreading throughout the world. In addition to this purpose, researchers are vigorously propelling the development of applications to various areas, such as NMR used for analysis, single-crystal pulling apparatuses, medical-purpose synchrotrons and cutting-edge medical equipment such as magnetoencephalographs.

In these applications at low temperatures, there is a possibility that the properties of high purity aluminium can be used effectively.

Conclusion

As described above, high purity aluminium is used as an industrial product for a wide range of purposes. In this paper we introduced such aluminium, mainly by focusing on its low-temperature properties and the refining technologies. Moreover, aluminium has other properties that can be improved by improving the purity. Thus its physical properties are being evaluated and its applications are being developed. Furthermore, due to the high purity aluminium-based alloying, uniquely special properties could be obtained. It is therefore expected that high purity aluminium can be applied in various areas. We want to understand the market needs precisely and will continue to develop materials in answer to such needs.

Lastly, we received tremendous support and guidance from Professor Tsunetaka Sumomogi at the Research Institute of Advanced Technology of Hiroshima Kokusai Gakuin University, and from Dr. Takayuki Tomaru and Dr. Kenichi Sasaki at the High Energy Accelerator Research Organization, Cryogenics Science Center. We hereby express our deep appreciation to them. Thank you very much.

References

- 1) H. Magusa, T. Satoh, A. Takahashi and H. Maeda, SUMITOMO KAGAKU, **1988-II**, 69 (1988).
- 2) M. Kondo, Y. Mizuno and H. Maeda, *Materia Japan*, **30** (1), 62 (1994).
- 3) S. Mikubo, *Aluminium*, **14**, (67), 19 (2007).
- 4) T. Sumomogi, M. Nakamura, M. Watanabe, H. Hiroaki, H. Tabuchi and H. Osono, *J. Japan Inst. Metals* **75** (10), 539 (2011).

- 5) T. Sumomogi, M. Nakamura, M. Watanabe, H. Hoshikawa, H. Tabuchi and H. Osono, *Materials Transactions*, **53** (06), 1084 (2012).
- 6) M. Nakamura, M. Watanabe, K. Tanaka, A. Kirihata, T. Sumomogi, H. Hiroaki and I. Tanaka, *J. Japan Inst. Metals* **77** (2), 44 (2013).
- 7) W. G. Pfann, "Zone Melting", Second Edition, John Wiley & Sons, Inc., New York (1958), p.8.
- 8) M. Miki and J. Takao, SUMITOMO KAGAKU, **1975-I** Special edition, 41 (1975).
- 9) O. S. Lutes and D. A. Clayton, *Physical Review*, **138**, A1448 (1965).
- 10) R. Stevenson, *Canadian Journal of Physics*, **45**, 4115 (1967).
- 11) K. T. Hartwig, G. S. Yuan and P. Lehmann, *Superconducting magnet Energy Storage (SMES), vol. 1: Basic R&D 1984-1985*, EPRI report GS-7053, (1990).
- 12) H. Hoshikawa, T. Megumi, H. Tabuchi, K. Sasaki, T. Tomaru and T. Shintomi, *Advances in Cryogenic Engineering*, **57**, 140 (2012).
- 13) S. Fujiwara, I. Nishino, S. Kuramochi, M. Otaki and C. Nagata, *Int. Conf. Process. Mater. Prop.*, **1**, 909 (1993).
- 14) Y. Ueda, *J. Sci. Hiroshima Univ., Ser. A*, **47**, 305 (1984).
- 15) I. Nakamichi and T. Kino, *Journal of Physical Society of Japan*, **49**, 1350 (1980).
- 16) K. Fuchs, *Proc. Camb. Phil. Soc.*, **34**, 100 (1938).
- 17) E. H. Sondheimer, *Adv. Phys.*, **1**, 1 (1952).
- 18) A. L. Woodcraft, *Cryogenics*, **45**, 421 (2005).
- 19) K. Kasahara, T. Tomaru, T. Uchiyama, T. Suzuki, K. Yamamoto, S. Miyoki, M. Ohashi, K. Kuroda and T. Shintomi, *TEION KOGAKU (J. Cryo. Super. Soc. Jpn.)* **39**, 25 (2004).
- 20) T. Tomaru, H. Hoshikawa, H. Tabuchi and T. Shintomi, *TEION KOGAKU (J. Cryo. Super. Soc. Jpn.)* **46**, 415 (2011).
- 21) Y. Makida, Y. Doi, T. Haruyama, K. Ten, H. J. Herman, M. Kawai, T. Kobayashi, T. Kondo, Y. Kondo, S. Mizumaki, G. Olesen, E. Sbrissa, A. Yamamoto and H. Yamaoka, *IEEE Transactions on Applied Superconductivity*, **12** (1), 407 (2002).
- 22) Y. Makida, T. Kumazawa, K. H. Tanaka, A. Yamamoto, T. Yoshida, S. Mizumaki and S. Kurita, *IEEE Transactions on Applied Superconductivity*, **15** (2), 1248 (2005).

PROFILE

*Hiroaki HOSHIKAWA*

Sumitomo Chemical Co., Ltd.
Basic Chemicals Research Laboratory
Research Associate

*Tomohiro MEGUMI*

Sumitomo Chemical Co., Ltd.
Basic Chemicals Research Laboratory
Researcher

*Ichiro TANAKA*

Sumitomo Chemical Co., Ltd.
Basic Chemicals Research Laboratory
Senior Research Associate
(Currently: Aluminium Division and Basic
Chemicals Research Laboratory)